

Vortex boundaries as barriers to diffusive vorticity transport in two-dimensional flows

Stergios Katsanoulis,¹ Mohammad Farazmand,² Mattia Serra,³ and George Haller^{1,*}

¹*Institute for Mechanical Systems, ETH Zurich, Leonhardstrasse 21, 8092 Zurich, Switzerland*

²*Department of Mathematics, North Carolina State University, 2311 Stinson Dr., Raleigh, NC 27695, USA*

³*School of Engineering and Applied Sciences, Harvard University, 29 Oxford Street, Cambridge, MA 02138, USA*

(Dated: October 17, 2019)

We put forward the idea of defining vortex boundaries in planar flows as closed material barriers to the diffusive transport of vorticity. Such diffusive vortex boundaries minimize the leakage of vorticity from the fluid mass they enclose when compared to other nearby material curves. Building on recent results on passive diffusion barriers, we develop an algorithm for the automated identification of such structures from general, two-dimensional unsteady flow data. As examples, we identify vortex boundaries as vorticity diffusion barriers in two flows: an explicitly known laminar flow and a numerically generated turbulent Navier–Stokes flow.

I. INTRODUCTION

Vortices in turbulent flows are omnipresent yet difficult to define unambiguously. As argued by [1], however, two common expectations for vortices have emerged in the literature: Material invariance and high levels of vorticity.

Regarding material invariance, Lugt [2] expects a vortex to be formed by material particles rotating around a common center, while McWilliams [3] requires a vortex to “persist under passive advection by the large-scale flow”. Chong et al. [4] view vortices as sets of instantaneously spiraling particle motions. Provenzale [5] emphasizes small material dispersion within vortex cores [6]. Chakraborty et al. [7] argue that both swirling motion and small particle dispersion are important features of a vortex core. Haller [8] views vortices as sets of non-hyperbolic trajectories and Chelton et al. [9] postulate that nonlinear eddies trap and carry fluid in their interior. In a similar setting, Mason et al. [10] seek vortices that are “efficient carriers of mass and its physical, chemical, and biological properties”.

Regarding vorticity in a vortex, McWilliams [3] and Hussein [11] expect high vorticity in vortices compared with the background flow. In contrast, Okubo [12], Hunt et al. [13], Weiss [14], Hua & Klein [15] and Hua et al. [16] require vorticity to dominate strain inside a vortex. Others compare vorticity to strain in the rate-of-strain eigenbasis [17] [18] [19]. Further variants of these ideas have been developed in the scientific visualization community, as reviewed in [20].

Formulating these guiding principles into a simple vortex definition has been a major challenge. At a conceptual level, the required material nature of the vortex necessitates an approach that truly targets material behavior. A litmus test for self-consistent material description is independence of the observer (or *objectivity*), which has long been enforced in continuum mechanics [21] [22] [23] for any theory purporting to describe material response. Objectivity was also identified as a basic requirement for flow feature detection in fluid mechanics already in the 1970’s [24] [25] [2], yet objective Lagrangian criteria for material vortex boundaries in two-dimensional flows have only appeared in recent years [26] [27] [1]. Of these approaches, only [1] involves the vorticity as a kinematic measure of rotational coherence. Seeking material regions from which vorticity transport is minimal, however, requires the involvement of the Navier–Stokes equations, an element that has been missing in the purely kinematic vortex criteria survived above.

More generally, finding theoretically optimal barriers to the transport of diffusive quantities in fluid flows has been an elusive problem (see, e.g., [28]). As a recent advance in this area, [29] formulated and solved a precise variational problem for material surfaces that inhibit the transport of weakly diffusive, passive scalar fields more than neighboring surfaces do in an incompressible flow. These results have subsequently been extended to compressible flows and to scalar fields with a known (and hence constrained) initial concentration [30].

Once a two-dimensional incompressible velocity field is known, its associated vorticity transport equation becomes a scalar advection-diffusion equation for the scalar vorticity. The initial condition of the equation, however, is constrained to be the plane-normal component of the curl of the velocity field at the initial time. Therefore, the general constrained transport barrier results of [30] apply to vorticity transport in incompressible, planar Navier–Stokes flows. We exploit this fact here and invoke the results of [30] to define and locate closed material curves that inhibit the leakage of vorticity from their interior most effectively.

* georgehaller@ethz.ch

We construct diffusive vortex boundaries as outermost periodic orbits of an explicit ordinary differential equation family arising from the exact solution to the minimal vorticity leakage problem. This automated algorithm is now publicly available under <https://github.com/katsanoulis/BarrierTool> in the MATLAB package entitled *BarrierTool*. We illustrate this algorithm first on an explicitly known solution of the planar Navier-Stokes equations, then on a two-dimensional decaying turbulence simulation.

II. CONSTRAINED MATERIAL BARRIERS TO VORTICITY TRANSPORT

As mentioned in the Introduction, Haller et al. [30] have derived the criteria for locating material barriers to diffusive transport in compressible flows. These results are applicable to arbitrary passive scalar fields in arbitrary spatial dimensions and with arbitrary diffusion tensors that possibly depend on space and time. Concentration sinks and sources, as well as spontaneous concentration decay are also allowed. Here we recall these results specifically formulated for the two-dimensional scalar vorticity field $\omega(\mathbf{x}, t)$ of an incompressible, two-dimensional Navier-Stokes velocity field $\mathbf{v}(\mathbf{x}, t)$ whose kinematic viscosity is $\nu \geq 0$.

In this context, if $\mathbf{v}(\mathbf{x}, t)$ is known, then $\omega(\mathbf{x}, t)$ satisfies the two-dimensional, linear advection-diffusion equation

$$\begin{aligned} \partial_t \omega + \nabla \omega \cdot \mathbf{v} &= \nu \Delta \omega, \\ \omega(\mathbf{x}, t_0) &= \omega_0(\mathbf{x}), \end{aligned} \quad (1)$$

where Δ is the Laplacian operator and ∇ denotes the gradient operation with respect to the spatial variable $\mathbf{x} \in U \subset \mathbb{R}^2$ on a compact domain U . We denote the flow map generated by the trajectories $\mathbf{x}(t; t_0, \mathbf{x}_0)$ of the velocity $\mathbf{v}(\mathbf{x}, t)$ by $\mathbf{F}_{t_0}^t(\mathbf{x}_0) := \mathbf{x}(t; t_0, \mathbf{x}_0)$. Consider an evolving material curve $\mathcal{M}(t) = \mathbf{F}_{t_0}^t(\mathcal{M}_0)$ with initial position $\mathcal{M}(t_0) = \mathcal{M}_0$. Let $s \in [\alpha, \beta]$ denote a parametrization of \mathcal{M}_0 and let $\mathbf{n}_0(s)$ denote a smooth unit normal vector field along \mathcal{M}_0 , and let $\Sigma_{t_0}^{t_1}(\mathcal{M}_0)$ denote the total normed transport of ω through the material curve $\mathcal{M}(t)$ over the time interval $[t_0, t_1]$. By normed transport we mean the time integral of the normed instantaneous flux, which therefore sums up all the leakage of ω through a curve without cancellations. The quantity $\Sigma_{t_0}^{t_1}(\mathcal{M}_0)$ is ideal for assessing the permeability of a surface for transport, whereas the unnormed (signed) vorticity transport may be small due to cancellations even for a highly permeable material curve. Note that both the normed and the unnormed vorticity transport are purely diffusive (i.e., vanish for $\nu = 0$), given that $\mathcal{M}(t)$ is a material surface and hence blocks all advective transport of a passive scalar field.

We are interested in finding initial curves \mathcal{M}_0 that extremize the normed and normalized vorticity transport functional

$$\tilde{\Sigma}_{t_0}^{t_1}(\mathcal{M}_0) := \frac{\Sigma_{t_0}^{t_1}(\mathcal{M}_0)}{\nu(t_1 - t_0) \int_{\mathcal{M}_0} ds},$$

where we have normalized the normed transport by the diffusivity, the length of the time interval and the length of the material curve \mathcal{M}_0 . As shown by [30], $\tilde{\Sigma}_{t_0}^{t_1}(\mathcal{M}_0)$ can be rewritten as

$$\tilde{\Sigma}_{t_0}^{t_1}(\mathcal{M}_0) = \frac{\int_{\mathcal{M}_0} |\langle \bar{\mathbf{q}}_{t_0}^{t_1}(\mathbf{x}_0(s)), \mathbf{n}_0(s) \rangle| ds}{\int_{\mathcal{M}_0} ds},$$

where $\mathbf{x}_0(s)$ denotes the parameterization of \mathcal{M}_0 ($s \in [\alpha, \beta]$) and the *transport vector field* $\bar{\mathbf{q}}_{t_0}^{t_1}(\mathbf{x}_0)$ is given by

$$\bar{\mathbf{q}}_{t_0}^{t_1}(\mathbf{x}_0) = \frac{1}{t_1 - t_0} \int_{t_0}^{t_1} [\nabla_0 \mathbf{F}_{t_0}^t(\mathbf{x}_0)]^{-1} [\nabla \omega(\mathbf{F}_{t_0}^t(\mathbf{x}_0), t)] dt, \quad (2)$$

where ∇_0 denotes the derivative with respect to \mathbf{x}_0 .

Material curves, $\mathcal{M}(t)$, that extremize $\tilde{\Sigma}_{t_0}^{t_1}$ have initial positions for which the variational derivative of $\tilde{\Sigma}_{t_0}^{t_1}$ vanishes,

$$\delta \tilde{\mathcal{E}}(\mathcal{M}_0^*) = 0. \quad (3)$$

Haller et al. [30] have obtained that the most observable class of solutions of this variational problem, *uniform vorticity barriers*, satisfy the conservation law

$$|\langle \bar{\mathbf{q}}_{t_0}^{t_1}(\mathbf{x}_0(s)), \mathbf{n}_0(s) \rangle| = \mathcal{T}_0, \quad 0 \leq \mathcal{T}_0 \leq \max_{\mathbf{x}_0 \in U} |\bar{\mathbf{q}}_{t_0}^{t_1}(\mathbf{x}_0)|, \quad (4)$$

for some constant \mathcal{T}_0 , which measures the pointwise constant, uniform transport density along such barriers. This conservation law gives an implicit differential equation for curve families $\mathbf{x}_0(s)$ that span initial positions of uniform material barriers to the diffusive transport of ω . Haller et al. [30] also show that an explicit differential equation family equivalent to the implicit one in (4) is given by

$$\mathbf{x}'_0 = \left(\mathcal{T}_0 \boldsymbol{\Omega} \pm \sqrt{|\bar{\mathbf{q}}_{t_0}^{t_1}(\mathbf{x}_0)|^2 - \mathcal{T}_0^2 \mathbf{I}} \right) \int_{t_0}^{t_1} [\nabla_0 \mathbf{F}_{t_0}^t(\mathbf{x}_0)]^{-1} \nabla \omega(\mathbf{F}_{t_0}^t(\mathbf{x}_0), t) dt, \quad \boldsymbol{\Omega} := \begin{pmatrix} 0 & 1 \\ -1 & 0 \end{pmatrix}. \quad (5)$$

Finally, Ref. [30] obtains a scalar diagnostic field, the *diffusion barrier strength* (DBS) field, that measures the local strength of transport barriers. This barrier strength is equal to the leading-order change in the local transport under small, localized normal perturbations to a transport barrier. The DBS field can simply be computed as

$$DBS_{t_0}^{t_1}(\mathbf{x}_0) = |\bar{\mathbf{q}}_{t_0}^{t_1}(\mathbf{x}_0)|, \quad (6)$$

with its ridges delineating the most influential vorticity transport extremizers. Both the exact differential equation (5) and the diagnostic field $DBS_{t_0}^{t_1}$ are objective, as shown by [30].

III. DIFFUSIVE VORTEX BOUNDARIES AS CLOSED MATERIAL BARRIERS TO VORTICITY TRANSPORT

The general equation (5) for planar vorticity barriers enables us to give a precise mathematical definition and a computational algorithm for diffusive vortex boundaries as most observable material inhibitors of vorticity leakage from a closed fluid region.

Definition 1. A *diffusive vortex boundary* over a time interval $[t_0, t_1]$ is a closed material curve $\mathcal{M}^*(t)$ whose initial position $\mathcal{M}_0^* = \mathcal{M}^*(t_0)$ is the outermost member of a closed orbit family in the differential equation family (5).

Each member of a periodic orbit family in (5) is technically a closed transport extremizer within its class. The orbit family as a whole provides an internal stratification of a vortical region into curves with the same uniform vorticity transport through them. The outermost member of such a family is the practically observed boundary of a region from which the leakage of vorticity is minimal, as shown in Fig. 1. The material curve $\mathcal{M}^*(t) = \mathbf{F}_{t_0}^t(\mathcal{M}_0^*)$ in Definition 1 is fully determined by its initial position \mathcal{M}_0^* , and hence the definition yields evolving material vortex boundaries $\mathcal{M}^*(t)$ over the whole time interval $[t_0, t_1]$. The pointwise strength of such a diffusive vortex boundary can then be assessed by computing $DBS_{t_0}^{t_1}(\mathbf{x}_0)$ along its points.

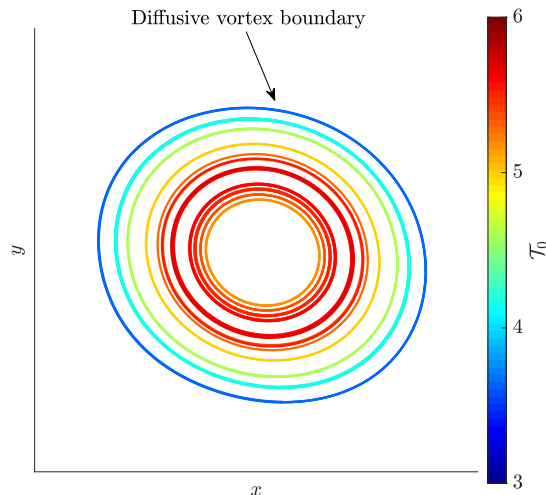


Figure 1. Family of limit cycles of equation 5. Each material curve has the same pointwise vorticity transport density \mathcal{T}_0 . The outermost member of this family serves as the diffusive vortex boundary.

Given that $\mathbf{n}_0(s) = \boldsymbol{\Omega} \mathbf{x}'_0(s) / \sqrt{\langle \mathbf{x}'_0(s), \mathbf{x}'_0(s) \rangle}$ is a smooth unit normal vector along any curve $\mathbf{x}_0(s)$, parametrized curves satisfying the conservation law (4) are also contained in the zero level set of the function family

$$L(\mathbf{x}_0, \mathbf{x}'_0; \mathcal{T}_0) = \sqrt{\langle \bar{\mathbf{q}}_{t_0}^{t_1}(\mathbf{x}_0), \Omega \mathbf{x}'_0 \rangle^2} - \mathcal{T}_0 \sqrt{\langle \mathbf{x}'_0, \mathbf{x}'_0 \rangle}, \quad (7)$$

which also turns out to be the Lagrangian associated with the variational problem (3) (cf. Ref. [30]). To locate closed zero-level curves of L , we adapt an idea originally developed in [31] for the automated computation of null-geodesics. First, we observe that the conservation law (4), and accordingly the zero level set of L , is invariant under reparametrizations of the curve $\mathbf{x}_0(s)$. This enables us to parametrize the yet unknown \mathcal{M}_0^* by arclength, i.e., for an appropriate angle $\varphi(s)$, we can set

$$\mathbf{x}'_0(s) = \mathbf{e}_\varphi(s) := \begin{pmatrix} \cos \varphi(s) \\ \sin \varphi(s) \end{pmatrix}, \quad \implies \mathbf{x}''_0 = \mathbf{e}_\varphi + \Omega^T \mathbf{e}_\varphi \varphi'. \quad (8)$$

Thus, by (7), curves in the zero level set of L satisfy

$$\sqrt{\langle \Omega \bar{\mathbf{q}}_{t_0}^{t_1}(\mathbf{x}_0(s)), \mathbf{e}_\varphi(s) \rangle^2} - \mathcal{T}_0 = 0. \quad (9)$$

Differentiating this last identity with respect to the parameter s and using the expression for \mathbf{x}''_0 from (8) gives

$$\langle \Omega \nabla_{\mathbf{x}_0} (\bar{\mathbf{q}}_{t_0}^{t_1}(\mathbf{x}_0)) \mathbf{e}_\varphi, \mathbf{e}_\varphi \rangle + \langle \bar{\mathbf{q}}_{t_0}^{t_1}, \mathbf{e}_\varphi \rangle \varphi' = 0. \quad (10)$$

Therefore, the definition of \mathbf{e}_φ in (8) and eq. (10) together yield an explicit, three-dimensional system of differential equations

$$\begin{aligned} \mathbf{x}'_0 &= \mathbf{e}_\varphi, \\ \varphi' &= \frac{\langle \Omega \nabla_{\mathbf{x}_0} (\bar{\mathbf{q}}_{t_0}^{t_1}(\mathbf{x}_0)) \mathbf{e}_\varphi, \mathbf{e}_\varphi \rangle}{\langle \bar{\mathbf{q}}_{t_0}^{t_1}(\mathbf{x}_0), \mathbf{e}_\varphi \rangle}, \end{aligned} \quad (11)$$

defined on the set $V = \{(\mathbf{x}_0, \varphi) \in U \times S^1 : \langle \bar{\mathbf{q}}_{t_0}^{t_1}(\mathbf{x}_0), \mathbf{e}_\varphi \rangle \neq 0\}$. Initial positions of closed material barriers to vorticity transport are closed projections of trajectories of (11) to the plane of the \mathbf{x}_0 variable.

IV. NUMERICAL ALGORITHM FOR DIFFUSIVE VORTEX-BOUNDARY DETECTION

Geometrically, the original variational problem (3) leads to a four-dimensional system of ODEs in the space of the $(\mathbf{x}_0, \mathbf{x}'_0)$ variables. The conservation law (4) enables us to reduce this four-dimensional ODE to the three-dimensional system (11). Note that if a trajectory of (11) projects to a closed curve $\mathbf{x}_0(s)$, then for any angle $\varphi_0 \in S^1$, there will be at least two points along the curve where $\mathbf{x}'_0 = \mathbf{e}_{\varphi_0} = (\cos \varphi_0, \sin \varphi_0)^T$. Therefore, for any choice of φ_0 , the set

$$\mathcal{C}_{\mathcal{T}_0} = \{(\mathbf{x}_0, \varphi) \in U \times \{\varphi_0\} : |\langle \bar{\mathbf{q}}_{t_0}^{t_1}(\mathbf{x}_0), \mathbf{e}_{\varphi_0} \rangle| = \mathcal{T}_0\}, \quad (12)$$

is a set of curves that all periodic orbits of (11) must cross. We can, therefore, use the set $\mathcal{C}_{\mathcal{T}_0}$ as a Poincaré section within each two-dimensional level set $|\langle \bar{\mathbf{q}}_{t_0}^{t_1}(\mathbf{x}_0), \mathbf{e}_\varphi \rangle| = \mathcal{T}_0$ to locate periodic orbits of (11). The trivial choice for the angle φ_0 is $\varphi_0 = 0$, in which case $\langle \bar{\mathbf{q}}_{t_0}^{t_1}(\mathbf{x}_0), \mathbf{e}_{\varphi_0} \rangle$ is simply the first component $[\bar{\mathbf{q}}_{t_0}^{t_1}(\mathbf{x}_0)]_1$ of the vector $\bar{\mathbf{q}}_{t_0}^{t_1}(\mathbf{x}_0)$ in the coordinate system selected for the analysis. These considerations lead to the numerical Algorithm 1 for locating diffusive vortex boundaries in a two-dimensional Navier–Stokes flow.

In our examples, we will use a MATLAB implementation of the above algorithm, which is publicly available under <https://github.com/katsanoulis/BarrierTool>. This MATLAB package *BarrierTool*, is in fact a more general software tool that allows for the computation of elliptic Lagrangian coherent structures [26], closed unconstrained diffusion barriers [29] and objective Eulerian coherent structures [32].

We note that a more technical, alternative approach to solving such variational problems involves a reduction of the original variational problem to a two-dimensional direction field family [30]. Locating closed curves of this direction field family involves the identification and analysis of direction field singularities. The associated challenges are described in [31] [33]. Recent progress on addressing some of these challenges is reported in [34].

Algorithm 1 Computing diffusive vortex boundaries

1. Input the 2D velocity field $\mathbf{v}(\mathbf{x}, t)$ defined over the spatial domain U and time interval $[t_0, t_1]$.
 2. Compute trajectories $\mathbf{x}(t; t_0, \mathbf{x}_0)$ of $\mathbf{v}(\mathbf{x}, t)$ over $[t_0, t_1]$, starting from an initial grid $\mathcal{G}_0 \subset U$.
 3. Calculate the deformation gradient $\nabla_0 \mathbf{F}_{t_0}^t(\mathbf{x}_0)$ for $\mathbf{x}_0 \in \mathcal{G}_0$ from finite differencing. Also, compute the vorticity gradient $\nabla \omega(\mathbf{x}, t)$ from finite differencing along each trajectory $\mathbf{x}(t; t_0, \mathbf{x}_0)$. Subsequently, compute the transport vector field $\bar{\mathbf{q}}_{t_0}^{t_1}(\mathbf{x}_0)$ and its gradient from finite differencing to obtain the right-hand side of (11) over the grid \mathcal{G}_0 .
 4. Fix a unit vector e_φ^0 and set up a loop over values of the transport density constant \mathcal{T}_0 falling in the interval given in (4).
 5. For each \mathcal{T}_0 value, calculate the initial condition set $\mathcal{C}_{\mathcal{T}_0}$ defined in (12) by computing the level set $|\langle \bar{\mathbf{q}}_{t_0}^{t_1}(\mathbf{x}_0), e_\varphi^0 \rangle| = \mathcal{T}_0$. Launch trajectories of the ODE (11) from $\mathcal{C}_{\mathcal{T}_0}$. For off-the-grid points in \mathcal{G}_0 , use bilinear interpolation to evaluate the right-hand side of eq. (11) for trajectory integration.
 6. Once the full loop of \mathcal{T}_0 is complete, identify diffusive vortex boundaries as the outermost members of the closed trajectory families obtained from the above procedure.
-

V. EXAMPLES

A. Periodic array of recirculation cells

A spatially periodic, steady solution of the 2D Euler equations is given by [35]

$$\mathbf{v}_E(\mathbf{x}) = 2 \begin{pmatrix} -2 \sin(2\pi x + 4\pi y) - \sin(4\pi x + 2\pi y) + \sin(4\pi x - 2\pi y) + 2 \sin(2\pi x - 4\pi y) \\ \sin(2\pi x + 4\pi y) + 2 \sin(4\pi x + 2\pi y) + 2 \sin(4\pi x - 2\pi y) + \sin(2\pi x - 4\pi y) \end{pmatrix}. \quad (13)$$

This Euler solution gives rise to the following spatially periodic, unsteady solution of the 2D Navier–Stokes equations

$$\mathbf{v}(\mathbf{x}, t) = e^{-20\pi^2 \nu t} \mathbf{v}_E(\mathbf{x}), \quad (14)$$

whose vorticity field

$$\omega(\mathbf{x}, t) = 20\pi e^{-20\pi^2 \nu t} [\cos(2\pi x + 4\pi y) + \cos(4\pi x + 2\pi y) + \cos(4\pi x - 2\pi y) + \cos(2\pi x - 4\pi y)]$$

satisfies the advection-diffusion equation (1) with viscosity ν .

The topology of the streamlines of the steady, inviscid velocity field $\mathbf{v}_E(\mathbf{x})$ is depicted in Fig. 2. The streamline geometry of the unsteady solution $\mathbf{v}(\mathbf{x}, t)$ remains the same. The central feature of this flow is delineated by the heteroclinic connections between the hyperbolic fixed points located at $(0, 0.5)$, $(0.5, 0)$, $(0, -0.5)$, $(-0.5, 0)$. This heteroclinic network encompasses an array of vortical recirculation regions around the elliptic fixed points located at $(0, 0)$ and $(e, 0)$, $(-e, 0)$, $(0, e)$, $(0, -e)$ with $e = \frac{1}{\pi} \arccos\left(\frac{\sqrt{6}}{4}\right)$. Furthermore, these vortical domains are separated from each other and from the outer heteroclinic network by an inner collection of heteroclinic connections among the hyperbolic fixed points located at (h, h) , $(-h, h)$, $(h, -h)$, $(-h, -h)$ with $h = \frac{1}{\pi} \arccos(\sqrt{\sqrt{6}/3 + 2/2})$.

All closed, periodic streamlines in the vortical regions are perceived as structures hindering the spread of high absolute vorticity from the centers of the vortical regions. Moreover, the periodic streamlines between the inner and the outer heteroclinic network should also be deemed as barriers to the transport of vorticity.

To verify this, we use Algorithm 1 to detect diffusive vortex boundaries based on Eq. (14) for two different integration times. As we observe in fig. 3, as the integration time $t_1 - t_0$ increases, the extracted diffusive vortex boundaries grow in number and size in the central elliptic region of high vorticity, whereas they become tighter around the four cores of high negative vorticity. Moreover, our algorithm captures larger diffusive vortex boundaries that closely align with both the inner and outer heteroclinic networks. Finally, we note the high correlation between the extracted diffusive vortex boundaries and the ridges of the DBS field.

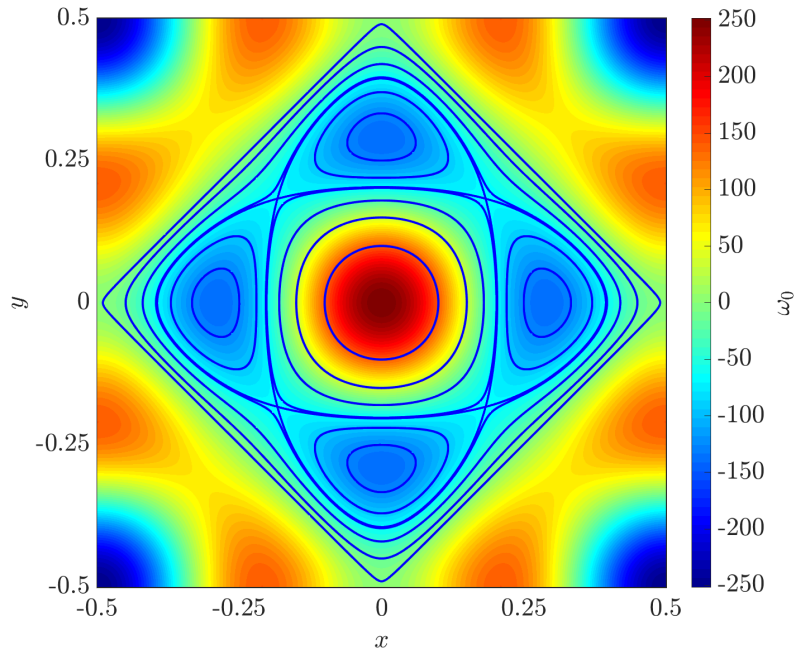


Figure 2. Streamlines of equation (14) with $\nu = 0.001$ at $t = 0$ overlaid on the initial vorticity field.

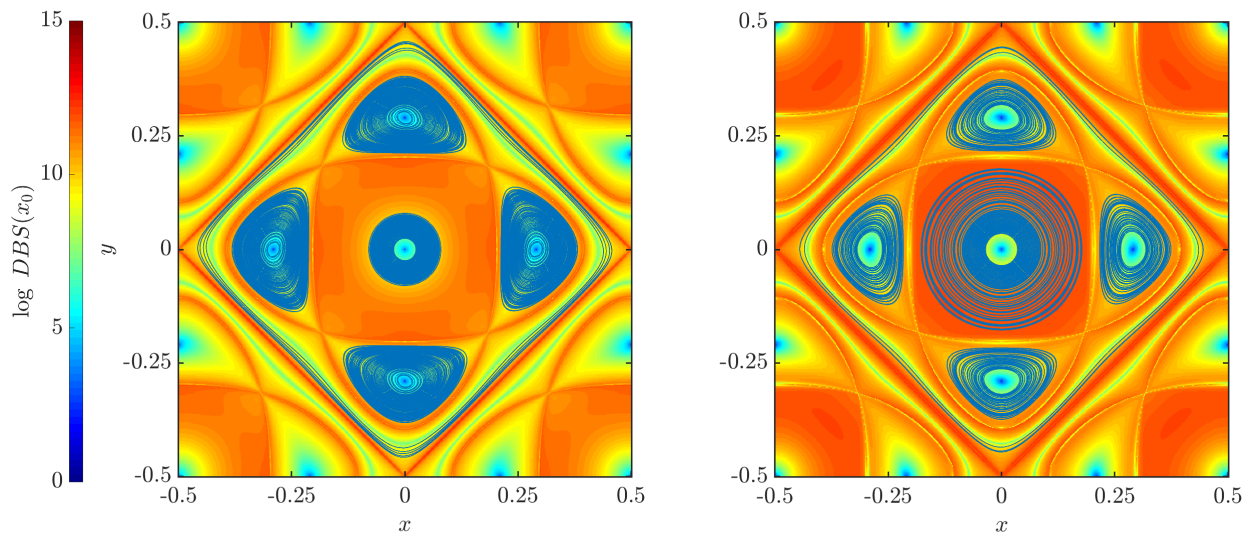


Figure 3. Barriers to vorticity transport (blue) superimposed on the $DBS_{t_0}^{t_1}(\mathbf{x}_0)$ field inside a vortex array of equation (14). The analysis was performed for $t_0 = 0$ and $t_1 = 1$ (left) and $t_1 = 5$ (right). In both cases, we set the kinematic viscosity $\nu = 0.001$.

B. Two-dimensional turbulence

We use a standard pseudo-spectral code to solve the two-dimensional, incompressible Navier-Stokes equations,

$$\partial_t \mathbf{v} + \mathbf{v} \cdot \nabla \mathbf{v} = -\nabla p + \nu \Delta \mathbf{v}, \quad \nabla \cdot \mathbf{v} = 0,$$

The domain is $[0, 2\pi] \times [0, 2\pi]$ with periodic boundary conditions. At Reynolds number $Re = \nu^{-1} = 5 \times 10^4$, the spatial coordinates are resolved using 1024^2 Fourier modes with 2/3 dealiasing. To construct the transport vector field, we advect trajectories from an initial grid of 1024×1024 points over the time interval $[0, 50]$. The Runge–Kutta algorithm of MATLAB (i.e., ode45) is used for the numerical integration. This algorithm uses an adaptive time stepping such that the relative and absolute errors are below 10^{-6} .

Fig. 4 shows different Lagrangian and Eulerian vortex identification methods for this computational experiment. In the entirety of fig. 4, we denote with red color the extracted diffusive vortex boundaries. For reference, we have also used BarrierTool to compute outermost material barriers to passive scalar diffusion [29], which are shown in yellow in fig. 4(a) as well as black-hole eddies [26], which are shown in yellow in fig. 4(b). Moreover, in fig. 4(c) we have identified Lagrangian-averaged vorticity deviation (LAVD) eddies using the parameter values described on [1]. For each of these plots the overlaid scalar fields correspond to the diagnostic field tied to the type of barriers that we have extracted (DBS, FTLE and LAVD, respectively). For all the Lagrangian vortex identification methods of fig. 4 we observe a clear correlation between all types of barriers, yet there are regions that only admit one kind of barrier but none of the others.

In addition, fig. 4(d) shows the negative Okubo-Weiss (OW) parameter field. The OW parameter is defined as

$$\text{OW}(\mathbf{x}, t) = s_2^2(\mathbf{x}, t) - \omega^2(\mathbf{x}, t) \quad (15)$$

where s_2 is the largest eigenvalue of the symmetric part of the velocity gradient. This quantity is broadly used in the literature to locate instantaneous vortical regions at domains where it attains negative values [12, 14].

Fig. 5 shows the final positions of the extracted diffusive vortex boundaries (red) and black-hole eddies (yellow) against the positions of an initially uniform grid of points color-coded with their DBS value. Black-hole eddies show no filamentation in agreement with their construction as locally minimally stretching coherent structures [26]. In contrast, diffusive vortex boundaries, constructed as extremizers to the transport of vorticity, manifest tangential stretching in some cases (blown up figures in Fig. 5). However, transport is still efficiently hindered by closed material curves that filament in tangential directions without a global breakaway that creates smaller scales. Moreover, the apparent dissimilarity in the detection of barriers in some regions is explained by the initial vorticity distribution (a constraint in our calculus of variations problem) which may tip the scales in favor of or against the detection of diffusive vortex boundaries irrespective of the existence of black-hole eddies.

The level curves of the OW parameter are often viewed as coherent structures in the flow [36]. We investigate this claim in fig. 6 which depicts a zoomed-in region close to the center of the computational domain along with an extracted diffusive vortex boundary, overlaid on level sets of the Okubo-Weiss (OW) parameter. In this region, $\text{OW}(\mathbf{x})$ signals two different vortical regions, while our algorithm only locates a material vortex boundary (as outermost barrier to vorticity transport) in one of these regions. To examine this prediction more closely, we compare the advected image of a set of tracers seeded along a level set of the $\text{OW}(\mathbf{x}, t)$ parameter against the final position of the diffusive vortex boundary. We observe that the material region obtained from our algorithm remains a coherent vortex that keeps vorticity concentrated. Over the same time interval, the material region surrounded by the OW level set completely falls apart, and hence this level set fails to prevent vorticity from leaking out from a coherent core.

Finally, the same image depicted in Lagrangian coordinates is shown in Fig. 7. More specifically, the norm of vorticity is portrayed as a surface over the Lagrangian coordinates \mathbf{x}_0 for two different configurations ($t_0 = 0$ and $t_1 = 50$). We observe that along the extracted diffusive vortex boundary vorticity is diffused in a uniform fashion which is in agreement with the underlying variational principle (minimal vorticity leakage) used in its construction. In contrast, the OW level set indicates no such organizing role in the vorticity landscape showing preferential directions along which vorticity diffuses more compared to the rest of the curve.

VI. CONCLUSIONS

We have proposed defining two-dimensional vortices as maximal regions enclosed by material barriers to the viscous transport of vorticity in Navier–Stokes flows. With this approach, we have been able to leverage the two-dimensional version of recent results of Haller et al. [30] on strongest material barriers to diffusion of a general passive scalar. We have used the conservation law provided by that theory to derive a three-dimensional, autonomous system of ODEs. Outermost closed projections of the orbits of this ODE onto the space of Lagrangian positions mark material curves satisfying our diffusive vortex boundary definition. Although not a part of the current work, a similar definition involving open solutions to the constrained barrier equations can be used to reveal signatures of material jet cores and fronts in the vorticity field. An extension of the present results to three dimensions, however, will require major modifications since three-dimensional vorticity is a vectorial quantity and no longer satisfies a linear advection-diffusion equation for a known velocity field.

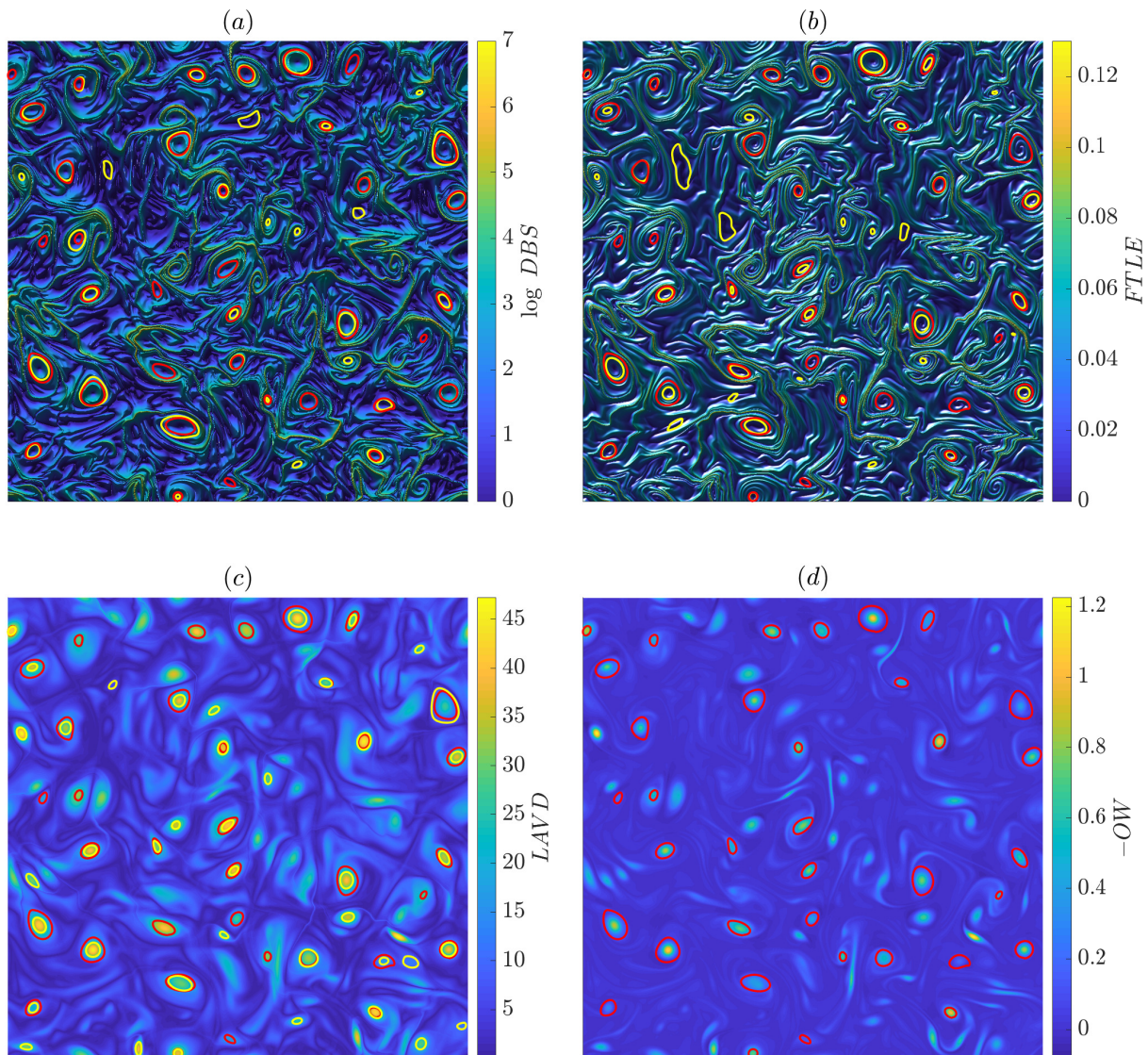


Figure 4. Lagrangian and Eulerian vortex identification methods on a decaying turbulence simulation with integration time $t_1 = 50$. (a) Diffusive vortex boundaries (red) and material diffusion barriers (yellow) superimposed with the $DBS_0^0(\mathbf{x}_0)$ field. (b) Diffusive vortex boundaries (red) and black-hole eddies (yellow) overlaid on the $FTLE(\mathbf{x}_0)$ field. (c) Diffusive vortex boundaries (red) and LAVD vortices (yellow) superimposed with the $LAVD(\mathbf{x}_0)$ field. (d) Diffusive vortex boundaries (red) overlaid on the negative Okubo-Weiss parameter field. All panels show the entire computational domain $[0, 2\pi] \times [0, 2\pi]$.

We have also introduced a numerical algorithm that automatizes the proposed vortex identification procedure. Upon comparing our algorithm with different Lagrangian vortex detection methods (geodesic theory of LCSs, LAVD, PRA) we find the present algorithm to be more computationally expensive owing to the need for computing the flow map gradient and the spatial derivatives of vorticity. At the same time, the proposed algorithm is objective (observer-independent), takes the Navier–Stokes vorticity dynamics into account, and requires no reliance on user input or heuristic parameters. Our open source MATLAB package, BarrierTool, provides a full implementation of the present results, as well as implementations of other Lagrangian vortex detection methods that are based on various material coherence principles.

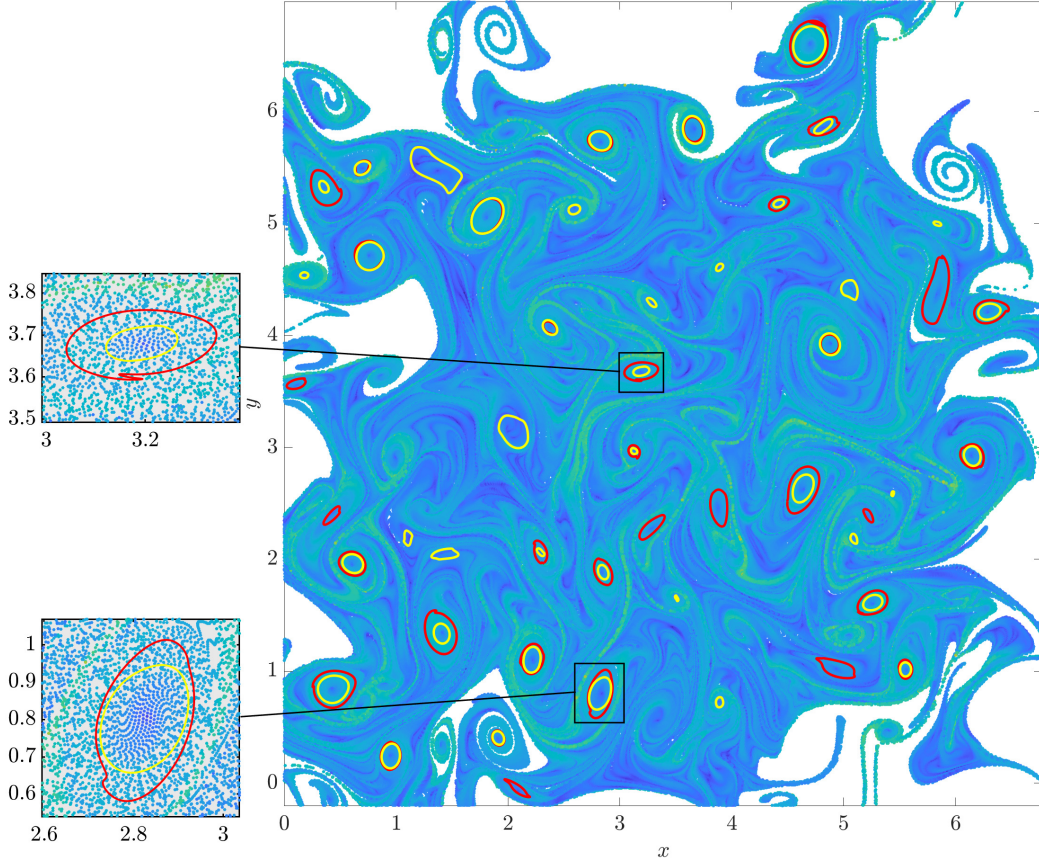


Figure 5. Final position at time $t_1 = 50$ of advected diffusive vortex boundaries (red) and black-hole eddies (yellow) overlaid on the advected position of a uniform grid of 500×500 tracers color-coded with their $\text{DBS}_0^{50}(\mathbf{x}_0)$ value. Close-ups: Tangential filamentation of the diffusive vortex boundaries in contrast to the unstretched black-hole eddies.

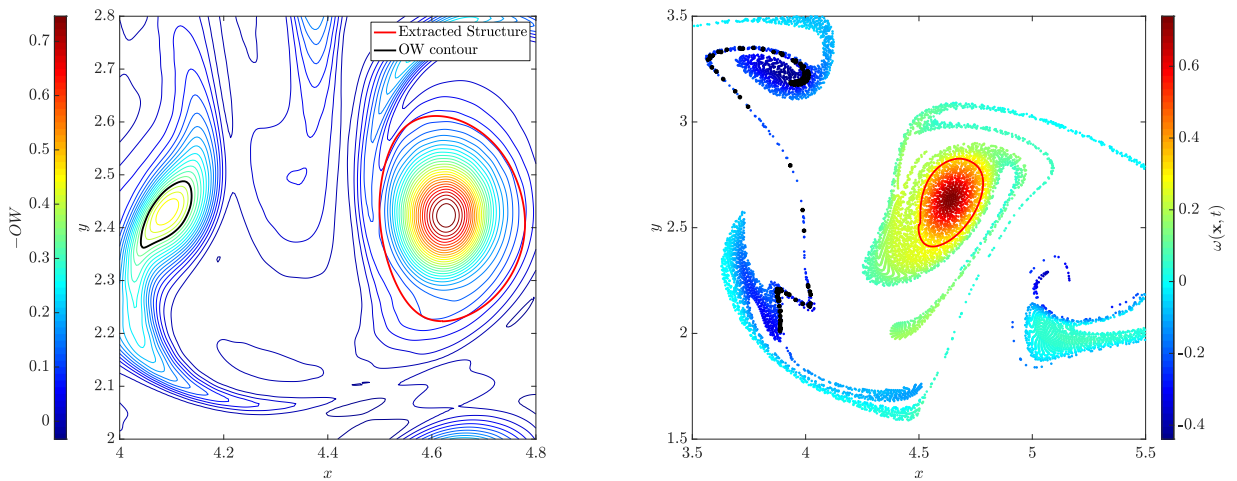


Figure 6. Left: Extracted diffusive vortex boundary (red) overlaid on level sets of the Okubo-Weiss (OW) parameter. Right: Advected image of the diffusive vortex boundary and a set of tracers lying initially on the black level set of the OW parameter superimposed with the final position of an originally uniform grid of points color-coded with their vorticity value.

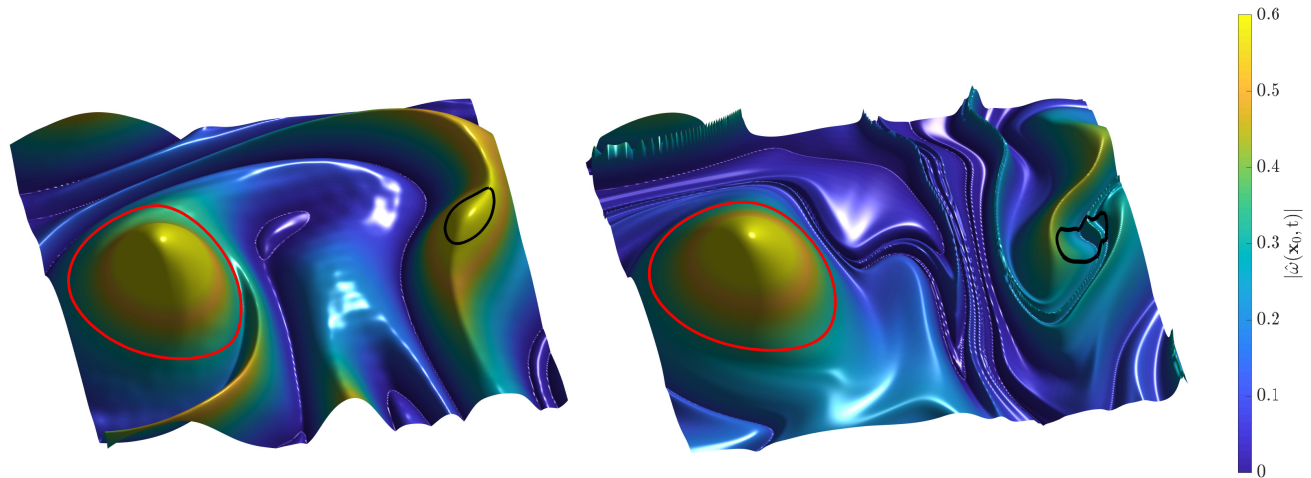


Figure 7. Evolution of $|\hat{\omega}(\mathbf{x}_0, t)|$, the vorticity norm in Lagrangian coordinates. Left: Colored contours of $|\hat{\omega}(\mathbf{x}_0, 0)|$ with the diffusive vortex boundary extracted from our algorithm (red) and OW level set (black). Right: Contours of $|\hat{\omega}(\mathbf{x}_0, 50)|$ with the same red and black curves at $t_1 = 50$.

ACKNOWLEDGMENTS

We are grateful to Daniel Karrasch and Hessam Babaei for useful discussions and comments. S.K. and G.H. acknowledge support from the Turbulent Superstructures priority program of the German National Science Foundation (DFG).

-
- [1] G. Haller, A. Hadjighasem, M. Farazmand, and F. Huhn, Defining coherent vortices objectively from the vorticity, *Journal of Fluid Mechanics* **795**, 136 (2016).
 - [2] H. J. Lugt, The dilemma of defining a vortex, in *Recent developments in theoretical and experimental fluid mechanics* (Springer, 1979) pp. 309–321.
 - [3] J. C. McWilliams, The emergence of isolated coherent vortices in turbulent flow, *Journal of Fluid Mechanics* **146**, 21–43 (1984).
 - [4] M. S. Chong, A. E. Perry, and B. J. Cantwell, A general classification of three-dimensional flow fields, *Physics of Fluids A: Fluid Dynamics* **2**, 765 (1990).
 - [5] A. Provenzale, Transport by coherent barotropic vortices, *Annual Review of Fluid Mechanics* **31**, 55 (1999).
 - [6] R. Cucitore, M. Quadrio, and A. Baron, On the effectiveness and limitations of local criteria for the identification of a vortex, *European Journal of Mechanics-B/Fluids* **18**, 261 (1999).
 - [7] P. Chakraborty, S. Balachandar, and R. J. Adrian, On the relationships between local vortex identification schemes, *Journal of fluid mechanics* **535**, 189 (2005).
 - [8] G. Haller, An objective definition of a vortex, *Journal of Fluid Mechanics* **525**, 1 (2005).
 - [9] D. B. Chelton, M. G. Schlax, and R. M. Samelson, Global observations of nonlinear mesoscale eddies, *Progress in Oceanography* **91**, 167 (2011).
 - [10] E. Mason, A. Pascual, and J. C. McWilliams, A new sea surface height–based code for oceanic mesoscale eddy tracking, *Journal of Atmospheric and Oceanic Technology* **31**, 1181 (2014).
 - [11] A. F. Hussain, Coherent structures and turbulence, *Journal of Fluid Mechanics* **173**, 303 (1986).
 - [12] A. Okubo, Horizontal dispersion of floatable particles in the vicinity of velocity singularities such as convergences, *Deep-Sea Research* **17**, 445–454 (1970).
 - [13] J. C. Hunt, A. A. Wray, and P. Moin, Eddies, streams, and convergence zones in turbulent flows, (1988).
 - [14] J. Weiss, The dynamics of enstrophy transfer in two-dimensional hydrodynamics, *Physica D* **48**, 273–294 (1990).
 - [15] B. Hua and P. Klein, An exact criterion for the stirring properties of nearly two-dimensional turbulence, *Physica D: Nonlinear Phenomena* **113**, 98 (1998).
 - [16] B. L. Hua, J. C. McWilliams, and P. Klein, Lagrangian accelerations in geostrophic turbulence, *Journal of Fluid Mechanics* **366**, 87 (1998).
 - [17] M. Tabor and I. Klapper, Stretching and alignment in chaotic and turbulent flows, *Chaos, Solitons & Fractals* **4**, 1031 (1994).

- [18] G. Lapeyre, P. Klein, and B. Hua, Does the tracer gradient vector align with the strain eigenvectors in 2d turbulence?, *Physics of fluids* **11**, 3729 (1999).
- [19] G. Lapeyre, B. Hua, and B. Legras, Comment on “finding finite-time invariant manifolds in two-dimensional velocity fields”[chaos 10, 99 (2000)], *Chaos: An Interdisciplinary Journal of Nonlinear Science* **11**, 427 (2001).
- [20] T. Günther and H. Theisel, The state of the art in vortex extraction, in *Computer Graphics Forum*, Vol. 37 (Wiley Online Library, 2018) pp. 149–173.
- [21] C. Truesdell and W. Noll, The non-linear field theories of mechanics, in *The non-linear field theories of mechanics* (Springer, 2004) pp. 1–579.
- [22] M. E. Gurtin, *An introduction to continuum mechanics*, Vol. 158 (Academic press, 1982).
- [23] M. E. Gurtin, E. Fried, and L. Anand, *The mechanics and thermodynamics of continua* (Cambridge University Press, 2010).
- [24] R. Drouot, Définition d’un transport associé à un modèle de fluide du deuxième ordre. comparaison de diverses lois de comportement, *CR Acad. Sci. A Math* **282**, 923 (1976).
- [25] R. Drouot and M. Lucius, Approximation du second ordre de la loi de comportement des fluides simples. lois classiques déduites de l’introduction d’un nouveau tenseur objectif, *Archiwum Mechaniki Stosowanej* **28**, 189 (1976).
- [26] G. Haller and F. J. Beron-Vera, Coherent lagrangian vortices: The black holes of turbulence, *Journal of Fluid Mechanics* **731** (2013).
- [27] M. Farazmand and G. Haller, Polar rotation angle identifies elliptic islands in unsteady dynamical systems, *Physica D: Nonlinear Phenomena* **315**, 1 (2016).
- [28] J. B. Weiss and A. Provenzale, *Transport and mixing in geophysical flows*, Vol. 744 (Springer, 2007).
- [29] G. Haller, D. Karrasch, and F. Kogelbauer, Material barriers to diffusive and stochastic transport, *Proceedings of the National Academy of Sciences* **115**, 9074 (2018).
- [30] G. Haller, D. Karrasch, and F. Kogelbauer, Material barriers to diffusive and stochastic transport in compressible flows, to appear in *SIAM j. Appl. Dyn. Sys.* (2019).
- [31] M. Serra and G. Haller, Efficient computation of null geodesics with applications to coherent vortex detection, *Proc. R. Soc. A* **473**, 20160807 (2017).
- [32] M. Serra and G. Haller, Objective eulerian coherent structures, *Chaos: An Interdisciplinary Journal of Nonlinear Science* **26**, 053110 (2016).
- [33] D. Karrasch, F. Huhn, and G. Haller, Automated detection of coherent lagrangian vortices in two-dimensional unsteady flows, *Proceedings of the Royal Society A: Mathematical, Physical and Engineering Sciences* **471** (2015).
- [34] D. Karrasch and N. Schilling, Fast and robust computation of coherent lagrangian vortices on very large two-dimensional domains, arXiv preprint arXiv:1907.08449 (2019).
- [35] A. Majda and A. Bertozzi, *Vorticity and incompressible flow*, Vol. 27 (Cambridge University Press, 2002).
- [36] Y. Dubief and F. Delcayre, On coherent-vortex identification in turbulence, *Journal of Turbulence* **1** (2000).